



CHALMERS
UNIVERSITY OF TECHNOLOGY

Impact of random packing on residence time distribution of particles in bubbling fluidized beds: Part 2 - Counter-current flow reactors

Downloaded from: <https://research.chalmers.se>, 2026-05-13 01:12 UTC

Citation for the original published paper (version of record):

Nemati, N., Mattisson, T., Pallarès, D. et al (2025). Impact of random packing on residence time distribution of particles in bubbling fluidized beds: Part 2 - Counter-current flow reactors. *Powder Technology*, 465.
<http://dx.doi.org/10.1016/j.powtec.2025.121306>

N.B. When citing this work, cite the original published paper.



Impact of random packing on residence time distribution of particles in bubbling fluidized beds: Part 2 - Counter-current flow reactors

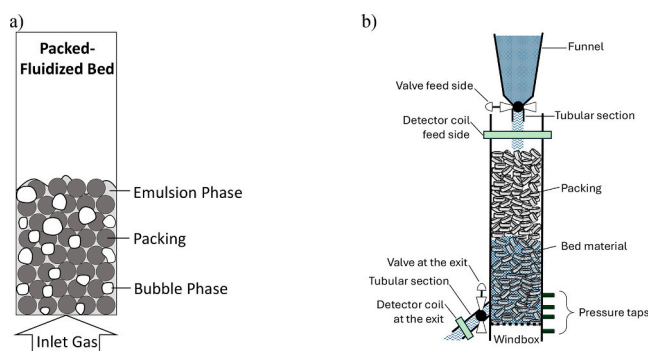
Nasrin Nemati^{*}, Tobias Mattisson, David Pallarès, Diana Carolina Guío-Pérez, Magnus Rydén

Division of Energy Technology, Department of Space, Earth and Environment, Chalmers University of Technology, Göteborg, Sweden

HIGHLIGHTS

- This study explores using packings in bubbling fluidized beds to enhance flow behavior toward plug flow reactor
- Packings reduce particle mixing effectively within the fluidized bed reactor system
- With packings, residence time curves resemble Gaussian shape, mimicking plug flow behavior
- Axial dispersion and tank-in-series models are used to categorize flow patterns of particles in the packed-fluidized beds
- Packings raise tank count and lower vessel dispersion number in bubbling bed compared to unpacked beds

GRAPHICAL ABSTRACT



ARTICLE INFO

Keywords:

Bubbling fluidized bed
Counter-current flow
Confined fluidization
Packed-fluidized bed
Residence time distribution
Magnetic solids tracing

ABSTRACT

The influence of employing random packings on the residence time distribution of bed solids in a counter-current bubbling fluidized bed is investigated. Magnetic solids tracing experiments have been performed in a bubbling fluidized bed setup (0.12 m in diameter) that allows for a continuous solids throughflow downwards. Two types of packings, aluminum silicate balls (ASB) and expanded clay aggregate (ECA) are employed in the experiments. Besides the effect of the packing type, the impact of fluidization number (15.6 and 21.9), and bed height (30 cm and 50 cm) are also studied. Two models are used to analyze the solids vertical flow patterns in the packed-fluidized beds, these are the axial dispersion and tank-in-series models. Findings indicate that the presence of packings provides the vertical throughflow of solids with a mixing pattern much closer to that of a plug-flow reactor, resulting in an increase in the Péclet number ($Pe = uL/D$) from 1.44 up to 18 and increasing the number of tanks by up to ninefold. The axial dispersion coefficient for the solids decreases almost tenfold (from approximately $0.06 \text{ m}^2/\text{s}$ in the unpacked bed to $0.006 \text{ m}^2/\text{s}$ in the packed-fluidized bed). The possibility of using packings to achieve plug-flow behavior of solids in a countercurrent fluidized bed could have positive implications for many current and future fluidized-bed conversion processes.

^{*} Corresponding author.

E-mail address: nasrinn@chalmers.se (N. Nemati).

<https://doi.org/10.1016/j.powtec.2025.121306>

Received 14 November 2024; Received in revised form 6 May 2025; Accepted 22 June 2025

Available online 23 June 2025

0032-5910/© 2025 The Authors. Published by Elsevier B.V. This is an open access article under the CC BY license (<http://creativecommons.org/licenses/by/4.0/>).

1. Introduction

In chemical engineering, plug flow reactors (PFR) and continuous stirred tank reactors (CSTR) represent two distinct ideal flow patterns of fluids. The defining characteristic of a PFR is the orderly flow of fluid through the reactor, devoid of any overtaking or mixing between consecutive elements in the direction of the flow. While lateral mixing may occur within a PFR, no mixing or diffusion occurs along the flow direction. The essential condition for plug flow is uniform residence time for all fluid elements [1,2]. In contrast, a CSTR maintains a state of thorough stirring and homogenous concentration, which ensures that the composition of the exit stream from the reactor mirrors that of the fluid within [1,2]. In reality, real reactors deviate from these idealized cases, necessitating investigation into parameters like the residence time distribution (RTD) and flow pattern, which are crucial for the design and optimization of reactors operation [1–3].

This study concerns fluidized bed reactors, the hydrodynamics of which have been studied extensively [4,5]. In fluidized bed reactors, two main phases exist: the bubble phase, mainly consisting of the fluidizing gas in the form of bubbles, and the emulsion phase, which contains both bed particles and gas. The movement of gas and solids in fluidized bed reactors is very complex, with the gas and solid generally exhibiting different types of flow behavior, and which is highly dependent on factors such as fluidizing velocity, particle size, and density [6–9]. Often referred to as fluidization regimes, flow behaviors range from fixed bed and bubbling bed reactors to turbulent and lean phase fluidization with pneumatic transport [6]. Understanding the flow patterns of solids and gases is crucial for the performance of many current and new energy conversion applications, including combustion, gasification and chemical-looping [10,11].

Two issues of central importance in the context of bubbling fluidized bed (BFB) reactors are: i) enhancing gas-solid contact in the reactor and ii) optimizing the flow pattern of the solids based on the reaction requirements. Both factors are important, as they largely govern the conversion of reactants. Below, a more detailed explanation of these issues is provided, as well as a review of the relevant literature findings.

In a BFB reactor with a well-mixed emulsion phase, bubble growth leads to a reduction in the surface area between the bubble and the emulsion phase. Consequently, the mass transfer rate of gas between these phases decreases as bubble size increases [11,12]. While small bubbles are desirable for effective mass transfer, large bubbles can have the opposite effect by causing gas bypass and slugging. Therefore, eliminating bubble growth is essential to enhance gas-solid contact and improve gas-solid mass transfer for applications that rely on this, such as chemical-looping processes or heterogeneous catalysis.

For other types of reactions in BFBs, such as equilibrium-controlled reactions where the solid and gas phase are in equilibrium, a well-mixed emulsion phase could limit the conversion of the final product, e.g. hydrogen production via the steam-iron process [13,14]. Understanding the flow patterns of solids and gases in such reactors with continuous solid flow is crucial for the performance of many fluidized bed applications. A fluidized bed exhibiting counter-current flow of fluid and solid particles would be valuable, for example, in applications such as temperature swing adsorption (TSA) processes, for instance, the adsorption of dilute carbon dioxide from flue gas streams [15–17]. Other example processes, as mentioned earlier, are the equilibrium reactions conducted in BFB, such as the steam iron reaction for H_2 production [18,19]. In this application, both H_2 yield (obtained by the oxidation of a reduced metal oxide with steam) and fuel conversion (obtained by the oxidation of a fuel by metal oxide) are thermodynamically limited, meaning that the conversion efficiencies of reactions is limited if the solid phase is well-mixed. Conducting these reactions in a scheme where the solids phase adopts a flow closer to PFR would be advantageous in shifting the equilibrium towards the desired products, similar to the counter-current moving flow pattern intended in moving beds. However, a counter-current moving bed arrangement would typically mean

employing very large particle sizes of around 1–2 mm [20].

To enhance efficiency for such processes, it is beneficial to create a progressive decrease in reactant concentration along the reactor's length. This can be achieved if the solids exhibit plug-flow behavior in the reactor. There have been several approaches to accomplishing this, including use of moving bed reactors with large particle sizes [20–22]. A way to shift the solids flow towards PFR is to decrease the cross section of the solids flow: this increases the mean axial velocity of the solids and the length they must flow through, both contributing to a higher Péclet number ($Pe = uL/D$), i.e. a stronger convective movement of the solids in comparison to the dispersive one associated with mixing. However, this approach presents certain limitations. Farha et al. [23] found that, for dense beds, reducing the cross section of solids flow yields an increased axial dispersion coefficient, D , due to the stronger frictional forces. Furthermore, smaller diameters may lead to hydrodynamic issues such as slugging, which are undesirable in BFB operation. Therefore, adjusting Pe is a strategy that requires careful consideration of design and operational parameters.

The concept of packed-fluidized bed or confined fluidization, illustrated in Fig. 1, involves the use of inert stationary random packings in a bubbling fluidized bed. Recent research by Nemati et al. [24–26] found a clear enhancing of the gas-solid contact in a BFB reactor when under packed-fluidized conditions.

Nemati et al. [24–26] applied different types of packings in BFB experiments and demonstrated that metal packings with high void factor, such as RMSR (stainless steel thread saddle rings) and Hiflow (stainless steel pall rings) with a void factor greater than 95 % effectively inhibit bubble formation and growth. This inhibition contributes to enhanced gas-solid contact efficiency and an improved fuel conversion rate compared to conventional BFB without packing in applications such as chemical-looping combustion. We hypothesize that the packed-fluidized bed concept can also be used to achieve a flow of solids closer to plug flow and will explore this idea in the current work.

Addressing the optimization of solid flow patterns, researchers such as Aronsson et al. [27] and Nemati et al. [28] conducted studies investigating solid throughflow in packed-fluidized beds using Aluminum silicate balls (ASB) with average diameters of 12.7 mm and 6.3 mm as the packing material. These packings had a lower void factor of less than 50 %, compared to RMSR or Hiflow. The measured solid flux in the ASB-

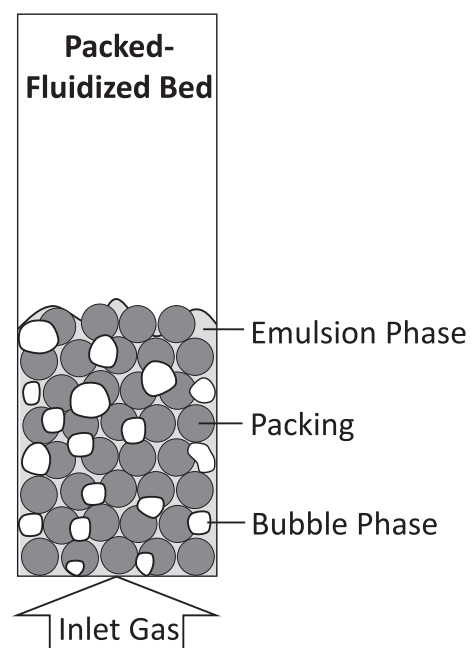


Fig. 1. Illustration of packed-fluidized bed (a.k.a. confined fluidized bed).

packed bed appeared significantly lower (ranging from 1.2 to 13.6 $\text{kgm}^{-2} \text{s}^{-1}$) than the solid flux desired in high-circulation applications like CLC (of up to 68.8 $\text{kgm}^{-2} \text{s}^{-1}$) [29]. As shown and discussed in previous work by the authors [27,28] the experimental set-up used was designed to maximize the width of the operation window, in which the solids-exit design was not limiting the solids flowrate. Instead, the solids flow rate was limited by resistance of the solids flow to enter the packed section from the top of packings, rather than hinderance inside the packed section (further details about the experimental setup can be found in references [27, 28]). However, the question was raised whether spherical packings could be of interest for applications benefiting from controlled solid flow patterns such as in PFR. This question underscores the importance of understanding the effect of spherical packings on BFB reactors with continuous throughflow of solids and their performance, emphasizing the need for more comprehensive investigations about this topic [28]. The reduction in axial solids mixing achieved through the introduction of these packings aims to transition the flow of solids from a well-mixed state towards plug flow. This shift would narrow the RTD of the solids, resulting in a more uniform output, which is essential for consistent performance in solids processing and throughput operations.

In this work, we aim to investigate whether packings can be used to modify the gas-solids flow in BFBs towards a more plug flow-like movement of the solids phase, i.e. reducing the mixing in the direction of the flow. Literature to date has underscored a general lack of comprehensive studies in this field [30], and the advance in energy technologies based on fluidized beds makes it important to further the knowledge-base in order to improve performance. This research is divided into two parts, focusing on two distinct flow configurations based on the relative directions of the gas and solids flows: cross-current flow and counter-current flow.

To achieve this objective, experiments are conducted in two different setups that allow continuous solids throughflow. The cross-current flow experiments in BFB reactors with continuous throughflow of bed material are detailed in the author's previous work, referred to as part 1 [31]. A schematic of the cross-current flow setup used in Part 1 is provided in the supplementary section (see Fig. S1 for more information). The results from part 1 show that the vessel's dispersion number for solids decreases in the presence of spherical packings compared to unpacked beds. Additionally, there is a noticeable shift in the RTD from the characteristics of a CSTR towards those of a PFR with axial dispersion in the packed-fluidized bed compared to an unpacked bed.

The present paper, referred to as part 2, aims to determine the influence of employing random packings on the solids' RTD and mixing in a BFB with counter-current flows of solids and gas. Experiments are conducted in a setup that allows continuous solids throughflow, examining the effects of different parameters such as packing type, gas velocity, and settled bed height.

2. Methodology

2.1. Experimental set-up

The experiments are performed in a cylindrical cold-flow fluidized bed which provides a counter-current flow of solids (downwards) and gas (upwards). The experiments are conducted at room temperature and atmospheric pressure. The setup with packings applied is illustrated in Fig. 2.

As shown in Fig. 2, the reactor consists of a cylindrical Plexiglas column with an inner diameter of 12 cm and a height of 1 m. Pressure is measured at four different positions. One pressure tap is located in the windbox. The three others are located 2.1, 7.6, and 13.2 cm above the gas distributor plate. Pressure is recorded using Huba Control transducers, digitalized through a NiDAQ A/D converter, and recorded with NI LabVIEW. The fluidizing gas is fed through a porous metal plate located at the top of the windbox. The air feed is regulated via LabVIEW, using Bronkhorst mass flow meters. A customized device is used to allow

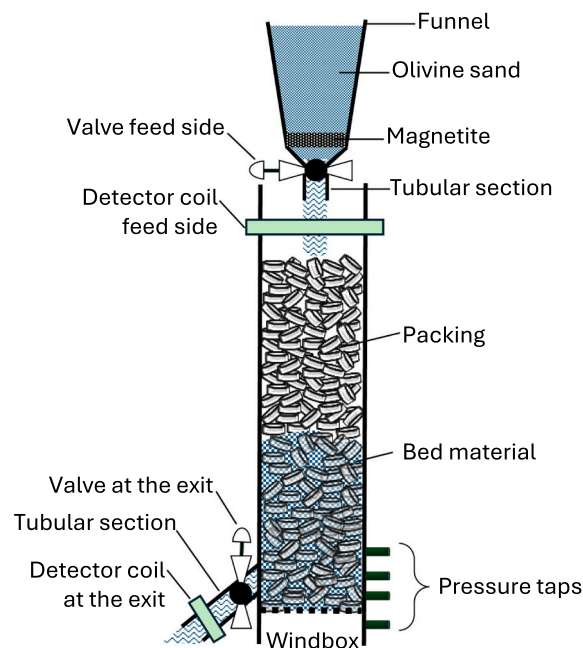


Fig. 2. The cylindrical laboratory-scale setup.

for the pouring of fluidizing solids at a constant rate on top of the reactor. It consists of a funnel-shaped reservoir with sharply inclined walls, where the bottom opening is attached to a ball valve. The valve is calibrated by measuring the time it takes to pour a certain mass of solids onto a scale. A known mass flow of solids, F_s (g/s), can thus be poured by adjusting the opening of the valve. At the bottom region of the cylindrical column, 35 mm above the distributor plate, an outlet pipe with an internal diameter of 30 mm and length of 75 mm is aligned with a 45° angle with respect to the reactor body. A ball valve is installed at the pipe's outlet to regulate the discharge rate of solid particles to match the solid mass flow rate, F_s (g/s), at the inlet. During operation, particles are consistently removed from the fluidized bed through the lower valve, while inert particles are introduced through the upper inlet valve located at the reactor's top. This setup allows for establishing a net counter-current flow of gas and solids.

The setup incorporates the magnetic tracer detection principle to measure particle RTDs. A custom-designed tracer detection device, inspired by the works of Guío-Pérez et al. [32] and Hofer et al. [30] is implemented. Coil inductors are employed to sense the concentration of magnetic tracer particles. More specifically, the change in the coils' inductance caused by the magnetic particles as they pass through the magnetic field of the coil sensor, can be correlated to the concentration of magnetic tracer in the sensed volume. As depicted in Fig. 2, a magnetic coil is placed at the feed side and another at the reactor's exit on the outlet pipe. It is important to note that solids located at different radial positions within the same height level near the column exit will exhibit varying exit times, as the exit is placed on the sidewall. The impact of this exit effect in the residence time distribution cannot be accurately measured for this setup configuration, but it is expected to widen the residence time distribution for all configurations. The alterations in inductance are recorded (50 Hz) and converted into concentration, following a previous calibration for the specific tracer material and coil geometry. This method allows to sample at a given location the transient concentration of ferromagnetic solids. In this work, the method is applied to track the transient outlet concentration of a pulsed batch of solids tracers especially chosen to mimic the fluid dynamics of the bulk solids. Thus, knowing the inlet time of the tracer batch, the residence time distribution of the tracer solids (and thus of the mimicked bulk solids) can be derived from the transient concentration of the batch at the outlet.

2.2. Bed material

The bed material and magnetic tracer utilized for the experiments are olivine sand and magnetite, respectively. The properties of the used materials are listed in Table 1. The chosen bulk material and tracer were selected to demonstrate optimal conformity in their fluid-dynamic properties, specifically ensuring similarity in the minimum fluidization velocity (u_{mf}). Both the bed material and the tracer fall under the classification of Geldart type B [7].

The minimum fluidization velocity, u_{mf} (m/s), is the velocity of the fluidizing gas at which the drag force exerted by the fluid on the particles balances the gravitational force acting on the particles, resulting in the fluidization of the bed. In this study, the correlation derived by Chitester et al. is applied to calculate u_{mf} (Eq. (1)) [6]. It is worth mentioning that the same correlation was used also in Part I of this study, which simplifies comparison.

$$\frac{d_p u_{mf} \rho_g}{\mu} = \left[(28.7)^2 + 0.0494 \times Ar \right]^{1/2} - 28.7 \quad (1)$$

where, Ar (–) is the dimensionless Archimedes number and is calculated through Eq. (2).

$$Ar = \frac{d_p^3 \rho_g (\rho_s - \rho_g) g}{\mu^2} \quad (2)$$

2.3. Packing material

Two types of packings are employed in the experimental investigations (Fig. 3): aluminum silicate balls (ASB) with an average diameter of 12.7 mm, and expanded clay aggregate (ECA) with an average diameter of 12 mm.

The determination of bulk densities for the respective packings involves loading a container of known volume and mass with packings. The bulk density is subsequently computed by dividing the increment in mass within the container with the packings by the container's volume. The void factor of packings, representing the fraction of unoccupied space within the packings, is assessed by employing the same empty container with a predetermined volume and mass. The container is initially filled with water, and the difference in mass is recorded. Following this, the container is emptied and filled with the packings. Subsequently, water is added until the container reaches full capacity, and the mass is recorded again. The void factor of the packings is calculated by dividing the masses obtained in these two measurements. Due to the low density of ECA packing and its potential for flotation upon water addition, as well as the porous nature of packings and the capacity for water absorption within their pores, the determination of the void fraction for both packings were conducted approximately ten times. The average bulk density and void factor values for both ASB and ECA packings are presented in Table 2.

2.4. Experimental procedure

This study explores and compares the response of a BFB with and

Table 1
Bed material and tracer properties.

Reactor type		Counter-current flow	
Material		Inert	Tracer
Properties	[unit]	Olivine Sand	Magnetite
d_p	μm	120	90
ρ_p	kg/m^3	2700	5100
ρ_b	kg/m^3	1603	2626
Ar	–	163	130
u_{mf}	m/s	0.016	0.017

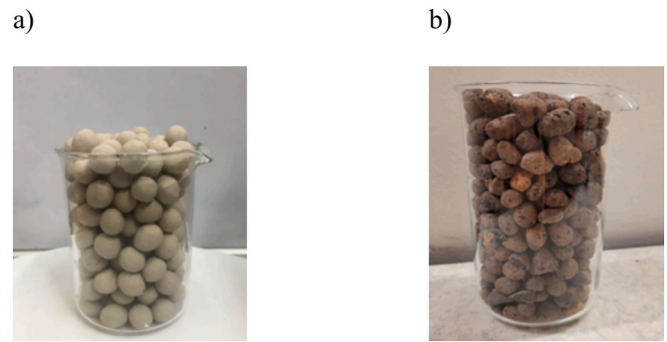


Fig. 3. Packings investigated in this work: a) ASB, b) ECA.

Table 2
Experimental determination of the properties of packings.

Packing	Bulk density [kg/m^3]	Void factor [–]
ASB	1400	0.45
ECA	280	0.58

without packing material to a pulse input of the tracer solids. In the experimental runs involving packing, the reactor is first filled with the specified packing material after which bulk solids are introduced up to a predetermined height within the packed zone, accompanied by the establishment of an airflow conducive to a bubbling regime. It should be noted that the height of packing materials was selected to be significantly greater than the bed material to prevent segregation caused by the likely higher flow rates of bed materials within the packed section [26]. Additionally, the packings remain static throughout the experiments.

Then, the inlet and exit valves of the reactor are adjusted to allow for a steady-state throughflow of bulk solids, confirmed by a constant solids inventory and monitored by measurement of the total pressure drop. Specifically, the pressure drop tracked is the difference between that in the windbox and the atmospheric pressure above the bed. This pressure drop across the bed is continuously checked to ensure its time-averaged value remains constant throughout the experiments, thereby ensuring a consistent bed height within the packed region as well as a consistent input and output of solids (further information can be found in Fig. S2 in the supplementary section). Upon this step, a small batch of tracer material ($m_t = 300$ g, representing 3.3–12.5 % of the bulk solids mass in the bed) is introduced upstream of the fluidized bed as a pulse input. This is done by adding the small batch of the tracer particles to the funnel above the top section (as illustrated in Fig. 2) while the steady throughflow of bed material is maintained. The termination criterion for the experiment is met when there is no longer any detection of tracer in the coil positioned at the exit of the reactor.

A series of experiments are conducted, varying the type of packing material, the superficial gas velocity, and the bed height. Table 3 presents the detailed test matrix for the experiments.

The dimensionless fluidization number, F (–), in Table 3 represents the ratio between the superficial gas velocity and u_{mf} (m/s). As shown in Table 3, two different settled bed heights and superficial gas velocities are established for each condition (packed bed and unpacked bed). However, the inlet and exit valves of the reactor are adjusted in order to maintain a constant solids throughflow rate of 68 g/s in all cases, regardless of the bed height.

2.5. Data evaluation: calculation of the solids RTD

The distribution of times required by the solid particles to leave the vessel is called the RTD or the exit age distribution E (s^{-1}) curve. The E -curve corresponds to the normalized time distribution, so the area

Table 3
Test matrix.

No.	Packing			Bed inventory			Air flow	
	Type	Packing void factor[-]	Packing height [cm]	Mass of Olivin sand in the bed (m_s) [kg]	Settled bed height [cm]	Solids flow (F_s) [g/s]	Superficial gas velocity [m/s]	Fluidization number (F) [-]
1	No packing	1	–	5.4	30	68	0.25	15.6
2	No packing	1	–	5.4	30	68	0.35	21.9
3	No packing	1	–	9.1	50	68	0.25	15.6
4	ASB	0.45	70	2.4	30	68	0.25	15.6
5	ASB	0.45	70	2.4	30	68	0.35	21.9
6	ASB	0.45	70	4.0	50	68	0.25	15.6
7	ECA	0.58	70	3.1	30	68	0.25	15.6

beneath the curve equals unity [1,2].

$$\int_0^\infty E(t) dt = 1 \quad (3)$$

In this study, a pulse input of the ferromagnetic tracer to the fluidized bed is used to determine the RTD of the solids. The normalized detected tracer concentration leaving the reactor, $C_{response}$ (-), is used for analyses. It is assumed that the injection is ideal, meaning it is a Dirac delta pulse. The E-curve is determined with Eq. (4) [1,2].

$$E(t) = \frac{C_{response,t}}{\sum_t C_{response,t} \Delta t_i} \quad (4)$$

As mentioned in section 2, the sampling frequency is 50 Hz, i.e. $\Delta t_i = 0.02$ s.

The dimensionless residence time distribution (RTD) function, E_θ , is a valuable metric when systems of different sizes are compared. In this study, the initial bed height is maintained constant for both packed and unpacked beds, resulting in significantly less bed material being present in the packed cases. Consequently, the overall mean residence time of the particles differs between the studied cases, with the packed-fluidized bed cases exhibiting shorter mean residence times for the same particle inlet flow rate. The dimensionless E-curve, E_θ , plotted against dimensionless time, θ , is thus used to normalize and compared solids flow behavior and effectively illustrates the changes in the RTD patterns between packed and unpacked fluidized beds (Eqs. (5, 6)).

$$E_\theta(\theta) = \tau E(t) \quad (5)$$

where

$$\theta = \frac{t}{\tau} = t \frac{\int_0^\infty C_{response,t} dt}{\int_0^\infty t C_{response,t} dt} \quad (6)$$

In this investigation, an assumption is made regarding the existence of a degree of plug flow at the entrance and exit of the vessels. This is, from the boundaries of the main vessel to the positions of the detection coils. This assumption stems from the configuration of the experimental reactor. Given the small diameter of the inlet and outlet pipes connected to the reactor, the mixing of bed materials within these regions is constrained. Consequently, the flow can be assumed to maintain a plug flow characteristic as it goes through these boundaries, referred to as closed boundary conditions or a closed vessel configuration (Fig. 4).

For a vessel with closed boundary conditions, the E-curve can be transformed into an alternative cumulative dimensionless format known as the F-curve (Eq. (7)).

$$F = \int_0^t E dt \quad (7)$$

The F(t) curve shows the fraction of particles which have been in the reactor for less than time t.

The measurement coils exhibit noise. A primary cause of this noise in

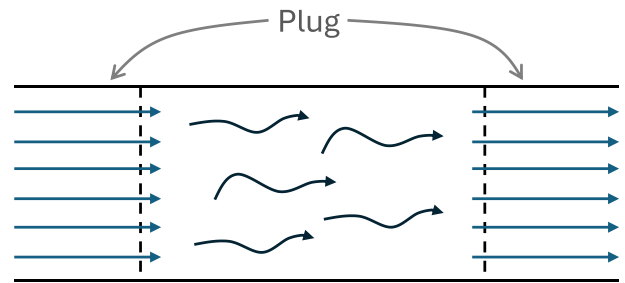


Fig. 4. Vessel with closed boundary conditions.

the outflow signals may be attributed to the nature of the outflow stream. The reactor's outflow is not consistently uniform and occasionally exhibits pulsing behavior, which can account for the observed noise in the signal curves. Thus, in this study, the raw signals are first filtered using a moving average function with a window size of 100 data points (equivalent to 2 s). Then, the parameters listed in Table 4 are evaluated for the conditioned response signal (the one acquired from the coil located at the outlet).

3. Modeling

Different models exist to categorize flow patterns based on their proximity to the ideal flow patterns (PFR, CSTR). The axial dispersion model and the tanks-in-series model are introduced in this section to assess deviations from plug flow in reactors.

3.1. Dispersion model

When a diffusion-like process is imposed on a plug flow, it is termed axial or longitudinal dispersion. The axial dispersion coefficient, D (m^2/s), characterizes the extent of this spreading phenomenon. A higher D signifies rapid spreading of the tracer, while a lower D indicates slower spreading, and $D = 0$ corresponds to no spreading, representing PFR. The dimensionless group D/uL , known as the vessel dispersion number,

Table 4
Characteristic values of the FB reactor determined from the coil response.

Parameter	Unit	Definition
$\tau_0 = 0$	S	Beginning of each experiment at which the tracer is injected into the FB.
τ_1	S	Time lag until the first detection of the tracer at the outlet coil.
$\tau = \frac{\int_0^\infty t C dt}{\int_0^\infty C dt}$	S	Mean residence time of tracer in the FB.
$\tau_{hyd} = \frac{m_s}{F_s}$	S	Hydraulic mean residence time of tracer in the FB.

quantifies the spread throughout the entire vessel. Notably, D/uL and Péclet number (Pe) are inversely related (Eq. (8)).

$$Pe = \frac{uL}{D} \quad (8)$$

where, L (m) is the characteristic length, representing the distance between the two designated measurement locations positioned at the entrance and exit of the fluidized bed (FB). Meanwhile, u (m/s) is the velocity of the solids traveling between these two measurement points ($L = 1$ m). Understanding the Pe number's definition reveals that a high Pe (> 1) in a reactor brings it closer to PFR behavior, while values $<< 1$ resemble patterns closer to a CSTR.

The Pe value can be evaluated through examining the variance of the tracer outlet concentration curve, σ^2 (s^2). Namely, considering a plug flow outside the vessel up to the boundaries (so-called closed boundary condition), the relationship between the variance of the tracer outlet concentration and Pe can be expressed as follows for Pe within 1–100 [1]:

$$\sigma_{\theta}^2 = \frac{\sigma^2}{\tau^2} = 2\left(\frac{1}{Pe}\right) - 2\left(\frac{1}{Pe}\right)^2 [1 - e^{-Pe}] \quad 1 < Pe < 100 \quad (9)$$

The variance of the tracer outlet concentration is a measure of the spread of the solids between the measurements at the inlet and outlet of the vessel and is calculated as [1]:

$$\sigma^2 = \frac{\int_0^{\infty} (t - \tau)^2 C_{response,t} dt}{\int_0^{\infty} C_{response,t} dt} = \frac{\int_0^{\infty} t^2 C_{response,t} dt}{\int_0^{\infty} C_{response,t} dt} - \tau^2 \quad (10)$$

where

$$\tau = \frac{\int_0^{\infty} t C_{response,t} dt}{\int_0^{\infty} C_{response,t} dt} \quad (11)$$

3.2. The tanks-in-series model

The tank-in-series model is simple and can be used with any kinetics and flow pattern. In this model, it is assumed that a number of tanks of the same size are connected in series. Since all the tanks are assumed to have the same size, the residence time in each tank is the same. Each of these tanks is considered an ideal CSTR unit and represents a distinct portion or segment of the reactor. The determination of the number of tanks-in-series can be made in different ways. In the present study, the variance of the tracer curve, $\sigma_{\theta}^2(-)$, is employed to extract the information about the quantity of tanks, N ($-$), as:

$$\sigma_{\theta}^2 = \frac{1}{N} \quad (12)$$

To verify the accuracy of the N tanks in series as determined from σ_{θ}^2 in Eq. (12), the RTD expression derived by MacMullin and Weber [1] is applied. This allows for a comparison between the model-derived E_{model} -curve (Eq. (13)) and the E -curve obtained from the experimental data (Eq. (4)).

$$E_{model} = \frac{1}{\tau} \left(\frac{t}{\tau}\right)^{N-1} \frac{N^N}{(N-1)!} e^{-tN/\tau} \quad (13)$$

where, τ is the mean residence time of the tracer in the FB derived from Eq. (11).

4. Results

In this investigation, a non-reactive tracer was introduced into the system via a pulse input to examine the E -curve through its outlet response. Section 4 provides the results regarding the reactor behavior that can be derived from the analysis of the E -curve data.

4.1. Solids RTD curves

Fig. 5 illustrates an example of E -curve derived from raw data, as well as conditioned E -curve utilizing a moving average function over time for different scenarios of beds, both with and without packing.

As seen from the data in Fig. 5, the transient response of the outlet concentration for the bed without packing is closer to that of a CSTR (a wider distribution) than that with the insertion of packings, which brings the response profile closer to the expected from a PFR (a narrower distribution). Fig. 6 illustrates the F -curves derived from the underlying raw data shown by the E -curves in Fig. 5.

As depicted in Fig. 5 and Fig. 6, the incorporation of ASB and ECA packings within the BFB system significantly influences the particle behavior and RTD within the bed. In the bed without packing, tracer detection at the reactor outlet commences simultaneously with the injection of the pulse into the system at $\tau_0 = 0$ s. The solids tracer concentration profile at the outlet of the unpacked bed reaches its peak around 10 s (Fig. 5), gradually diminishing over a span of approximately 200 s, at which around 80 % of the tracer is evacuated from the reactor (Fig. 6). In contrast, when ASB and ECA packings are introduced into the reactor, the first tracer particles reach the outlet in approximately 8–15 s. Subsequently, the tracer peak is detected at the outlet within approximately 30 s (Fig. 5). After approximately 60 s, more than 80 % of the tracer has exited the reactor (Fig. 6). Thus, at an 80 % threshold, the span of tracer particles residence time within the FB is reduced from approximately 200 s to an average of 50 s in the presence of packings.

As discussed in section 3, the dimensionless E_{θ} function is an important tool for evaluating the cases with different overall mean residence time of the particles in the bed. Fig. 7 illustrates conditioned E_{θ} -curve with a moving average function over dimensionless time, θ , for the beds with and without packing.

Fig. 7 shows that the inclusion of ASB and ECA packings make the E_{θ} -curve narrower and shift the peak towards $\theta = 1$. This indicates that the mean of the data aligns with the mode, suggesting a more symmetric distribution. Thus, the packings reduce vertical particle mixing in the reactor, resulting in a behavior more similar to that of a PFR with axial dispersion. Conversely, the absence of packing material in the system aligns its behavior more closely with that of a CSTR (Further information about E -, F - and E_{θ} -curves of other operating conditions can be found in Fig. S3–S4 in the supplementary section).

Results of different operational conditions are compiled in Table 5, including the mean residence time of the tracer within the FB, τ , and the time interval between tracer injection at $\tau_0 = 0$ s, and the detection of the initial tracers exiting the FB at τ_1 . The variation of τ and τ_1 for the packed bed compared to the unpacked bed is also presented in Table 5.

As indicated in Table 5, the mean residence time of the tracer within

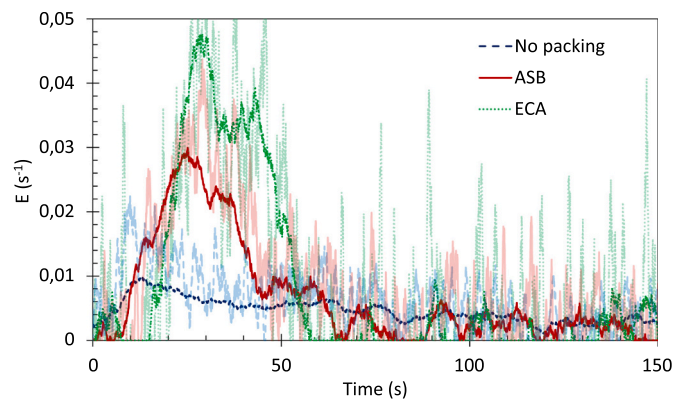


Fig. 5. E -curve as determined from the outlet concentration of tracers for the counter-current flow BFB: settled bed height $H = 30$ cm, fluidization number $F = 15.6$, solid throughflow $F_s = 68$ g/s, ($\tau_{No\ packing} = 110.4$ s, $\tau_{ASB} = 31.5$ s, $\tau_{ECA} = 34.1$ s).

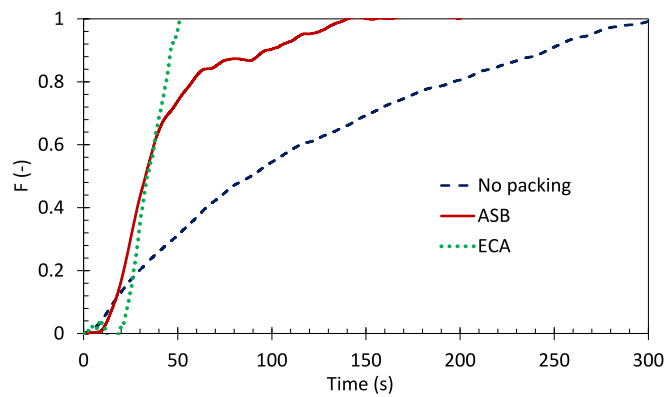


Fig. 6. F-curve at the outlet of counter-current flow BFB: settled bed height $H = 30$ cm, fluidization number $F = 15.6$, solid throughflow $F_s = 68$ g/s, ($\tau_{No\ packing} = 110.4$ s, $\tau_{ASB} = 31.5$ s, $\tau_{ECA} = 34.1$ s).

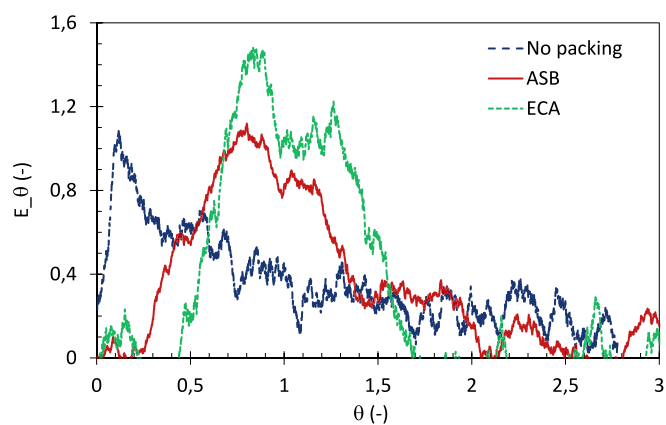


Fig. 7. E_0 -curve at the outlet of counter-current flow BFB: settled bed height $H = 30$ cm, fluidization number $F = 15.6$, solid throughflow $F_s = 68$ g/s.

Table 5

Mean residence time (τ) and time lag until the detection of the tracer (τ_1). Solids throughflow was kept constant at $F_s = 68$ g/s.

No.	Packing	Bed inventory	Air flow	Results		
	Type	H [cm]	$F = u/u_{mf}$ [-]	τ (variation vs no-packing) [s]	Time for first outlet detection, τ_1 [s]	$\tau_{hyd} = m_s/F_s$ [s] (variation compared to τ)
1	No packing	30	15.6	110.4 (-)	0	79.4 (-31)
2	No packing	30	21.9	56.3 (-)	0	79.4 (+23)
3	No packing	50	15.6	100.0 (-)	0	133.8 (-34)
4	ASB	30	15.6	31.5 (-78.9)	8	35.3 (-4)
5	ASB	30	21.9	39.5 (-16.8)	11	35.3 (+4)
6	ASB	50	15.6	51.4 (-48.6)	16	58.8 (-7)
7	ECA	30	15.6	34.1 (-76.3)	15	45.6 (-11)

the FB, τ , decreases in the bed containing ASB and ECA packings compared to unpacked beds at all the investigated conditions. This reduction reaches up to 71 % when packings are applied. Additionally, Table 5 provides data on the time lag until the first tracer detection at

the outlet, τ_1 , which increases in the range of 8–16 s when packings are used. This, together with the average residence time of the tracer inside the bed, suggests that the E-curve with packings approaches closer to a Gaussian shape, indicating that the system behavior aligns more closely with that of a PFR.

Another key observation from Table 5 is the difference between the mean residence time, τ , and the hydraulic residence time, τ_{hyd} . Ideally, these two values should be equal. Any difference between them suggests the presence of flow irregularities in the FB, such as dead zones, short-circuiting, bypassing, or back-mixing. As shown in Table 5, the difference between τ and τ_{hyd} reaches up to 34 s in the unpacked bed, whereas it remains below 11 s in the packed beds. Further discussion on the significance of these values can be found in other references [30, 33].

4.2. The dispersion and tanks-in-series models

To quantify the flow pattern of solids in the reactor, the dispersion model and tank-in-series models are applied to the experimental data. The objective of this modeling section is to compare the changes in the Pe , dispersion coefficient, and number of tanks in series when packings are used, against the bed without packings, and to highlight these differences.

Table 6 presents the parameters derived from counter-current flow experiments utilizing the dispersion and tank-in-series models. The results are presented for various fluidization numbers (F), bed heights (H), and types of packing materials. The Pe -values in Table 6 are calculated from Eq. (9), and with those the vertical dispersion coefficient for the solids throughflow can be calculated through Eq. (8).

As depicted in Table 6, the incorporation of ASB and ECA packings results in a significant increase in the Pe number, exceeding by up to eleven times the Pe values observed in unpacked beds. On the other hand, σ_θ^2 (-) is also an indicator of the dispersion of the E-curve and is calculated through Eqs. (9)–(11). Table 6 summarizes σ_θ^2 and N from the tanks-in-series model. A lower value of σ_θ^2 indicates decreased dispersion within the E-curve and lower degrees of scattering. Consequently, the reactor behavior tends towards resembling a PFR, leading to an increase in the number of theoretical tanks, N (-), required (Eq. (12)). Comparing the N values between experiments utilizing packings and those conducted with an unpacked bed in Table 6, under similar operating conditions, it is evident that the introduction of packings results in an increase in N by up to ninefold in comparison to the unpacked beds. Furthermore, when comparing cases with similar mean residence times (τ), such as cases 2 and 6 in Table 5, the use of packings (case 6) results in an N value up to ten times higher than that of the unpacked case (case 2). Consequently, the reactor's behavior in packed-fluidized bed converges towards that of a PFR characterized by higher Pe and N values.

Table 6

Parameters of dispersion and tank-in-series models for counter-current flow: for different F (-), H (cm), and packing type. Solids throughflow was kept constant at $F_s = 68$ g/s, yielding a solids superficial velocity of 0.1 m/s.

Case	Packing	Bed inventory	Air flow	Dispersion model		Tank in series model	
	Type	H [cm]	$F = u/u_{mf}$ [-]	Pe [-]	D [m^2/s]	σ_θ^2 [-]	N [-]
1	No packing	30	15.6	1.44	0.069	0.65	1
2	No packing	30	21.9	1.75	0.056	0.65	1
3	No packing	50	15.6	2.96	0.034	0.46	2
4	ASB	30	15.6	10.19	0.009	0.17	6
5	ASB	30	21.9	17.00	0.006	0.11	9
6	ASB	50	15.6	18.00	0.006	0.10	10
7	ECA	30	15.6	13.38	0.007	0.14	7

The differences between the flow pattern established with each of the two packing materials, ASB and ECA, were not significant under the studied conditions. Under similar operating conditions, (see cases 4 and 7 in Table 6), results indicate a reduction of 22 % in the axial dispersion coefficient for the ECA packing (which translates into an increase of one in the number of tanks-in-series).

Comparing cases 1 and 2 in Table 6, it is seen that an increase in the fluidization number, F , does not significantly influence the solids dispersion (and thus not either the Pe number) in a bed without packing. However, with the application of ASB packings (cases 4 and 5), the same increase in fluidization velocity yields a considerable decrease in solids dispersion (33 %, translating into the number of tanks increasing from 6 to 9).

An increase in bed height results in a more important role of the convective solids transport in front of the dispersive one (i.e. higher Pe -number and number of tanks), with this trend being more pronounced in packed-fluidized conditions (see cases 4 and 6) than under freely bubbling (see cases 1 and 3). This is expected since a higher bed increases the characteristic mixing length of the system, which provides worse conditions for the dispersive mixing to contribute.

In this section, the objective of employing the two distinct models—the dispersion model and the tanks-in-series model— was not to compare their performance to determine which is superior. Rather, it was to assess whether both models could adequately describe the system and highlight the differences between the packed bed and the unpacked bed. The conclusion remains consistent irrespective of the model used.

4.3. The E -curve for tanks-in-series model

The formulation of a model incorporating a series arrangement of CSTR is achieved through Eq. (13) (see section 4.2). The N from the tanks-in-series model and the mean residence time τ , from experiments are applied in this model to obtain and plot the RTD curve. The outcomes of this model for $F = 15.6$ and $H = 30$ cm are plotted and compared with the experimental results for the conditioned data with moving average function for all packed and unpacked beds, as illustrated in Fig. 8.

As seen in Fig. 8, the model demonstrated a very good fit for all examined scenarios. Furthermore, the model outcomes also confirm the notable differences in the N values between packed and unpacked fluidized beds, with estimated values of approximately 6 CSTRs for ASB, 7 CSTRs for ECA, and 1 CSTR for the unpacked bed. This observation suggests a substantial increase in the number of CSTRs by up to seven-fold for the packed bed configurations. These findings confirm the reliability and consistency of the analyses conducted through dispersion and tank-in-series models. Consequently, the operational characteristics of the BFB without packing approach those similar to a CSTR. Conversely, the introduction of packings in the BFB leads to a behavior more closely resembling that of a PFR.

The experimental and modeling results for the E -curve for the beds with ASB packings, with parameters $H = 50$ cm and $F = 21.9$ are depicted in Fig. 9.

The observations from Fig. 9 indicate favorable agreement between the model and experimental outcomes under varied conditions. Elevating both the fluidization number and bed height in a packed fluidized bed operating with a counter-current flow of solid material and fluidizing gas results in an increase in the number of tanks. Consequently, based on these findings, raising these parameters in a packed fluidized bed is poised to enhance the performance of the bed towards a closer resemblance to PFR behavior.

4.4. The summary of cross-current flow and counter-current flow experiments

This section aims to summarize and compare the results from Part 1 (cross-current flow), presented in the previous publication [31], and

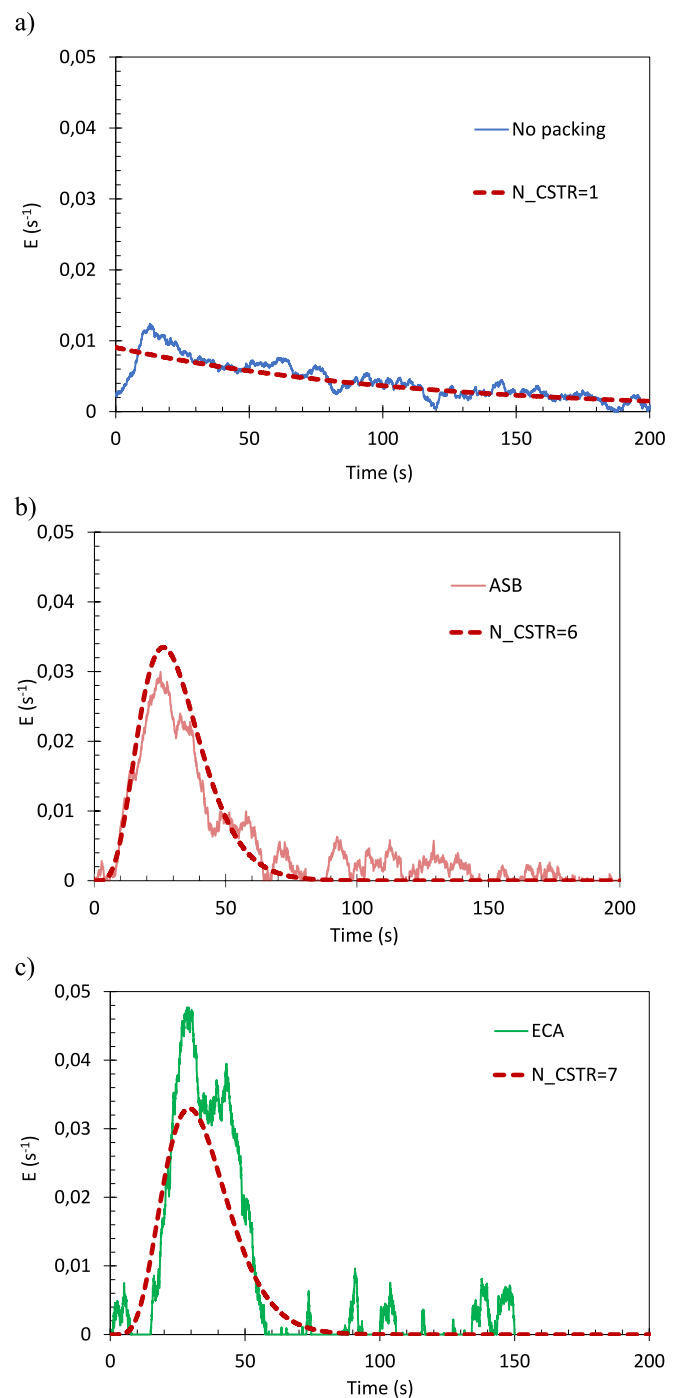


Fig. 8. Modeling results for E -curve of counter-current flow BFB as a function of time (Eq. (13)), fluidization number $F = 15.6$, bed height $H = 30$ cm, solid throughflow $F_s = 68$ g/s: a) No packing, b) ASB, c) ECA.

Part 2 (counter-current flow) from the current study, focusing on bubbling fluidized beds with and without packings. Table 7 provides the Pe numbers for both parts.

A general observation is that, for both cross-current and counter-current flow configurations, the Peclet (Pe) number remains at a maximum of 2 in the absence of packing. However, the introduction of packings in the fluidized bed significantly increases the Pe number, indicating a substantial influence of packings on solids flow patterns in both cases. Additionally, the effect of increasing the fluidization number (F) on the Pe number is noteworthy. In the counter-current reactor, an increase in F leads to a rise in the Pe number, whereas in the cross-

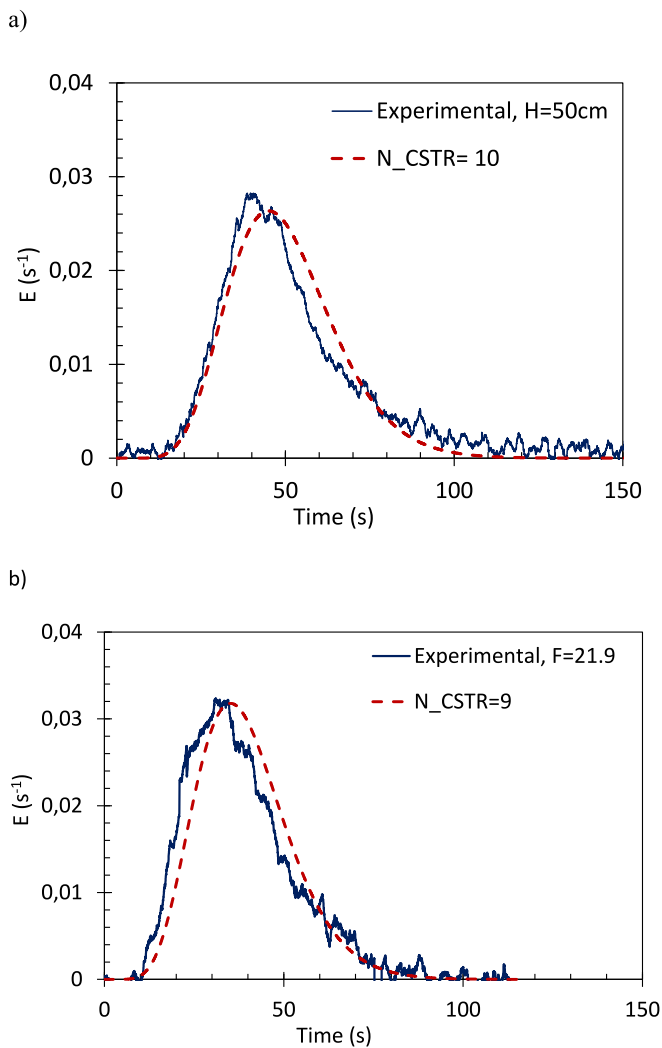


Fig. 9. E-curve of experimental results and the model for bed with ASB packing for conditioned signals with a moving average function: a) $H = 50$ c, $F = 15.6$, $F_s = 68$ g/s, b) $H = 30$ cm, $F = 21.9$, $F_s = 68$ g/s.

Table 7

The results of Pe -number for counter-current experiments with $H = 30$ cm and $F_s = 68$ g/s and for cross-current experiments with $H = 20$ cm, $F_s = 92$ g/s.

Flow pattern	Packing	Air flow	Dispersion model	Variation compared to non-packed bed
	Type	F [-]	Pe [-]	[-]
Counter-current	No packing	15.6	1.44	-
	No packing	21.9	1.75	-
	ASB	15.6	10.19	8.75
	ASB	21.9	17.00	15.25
	ECA	15.6	13.38	11.94
	No packing	8.8	2.13	-
Cross-current	No packing	6.6	1.99	-
	No packing	4.4	2.07	-
	ECA	8.8	4.15	2.02
	ECA	6.6	7.61	5.62
	ECA	4.4	8.81	6.74

current reactor, increasing F results in a decrease in Pe . This contrast is an important finding from these two studies.

5. Discussion

In a BFB, if the solid particles are continually added and removed from the reactor, it results in a net flow of solids. For example, if solids are added at the top and removed from the bottom of the fluidized bed, there would be a downward flow of solid particles counter-current to the upward flowing fluid. In this sort of fluidized beds, it is generally desirable to reduce channeling of the fluid through the solid particles and the formation of stagnant zones of fluid or solid particles within the bed. It is also desirable to minimize recirculation or back-mixing of the solid particles and fluid within the fluidized bed due to the detrimental effects back-mixing can have on the efficiency of the process. This type of fluidization is analogous to a PFR. A PFR facilitates a progressive decrease in reactant concentration along its length, making it more efficient for reactions where rate increases with reactant concentration, compared to a CSTR where concentration drops immediately to a low value [1,2].

This study is divided into two parts and examines the impact of packings on modifying the behavior of a bubbling fluidized bed (BFB) from CSTR-like to PFR-like for two different flow configurations. The first part [31] is conducted in a rectangular cuboid reactor that provides a cross-current flow of solids and gas, similar to the stages of a TSA column as described by Pröll et al. [15]. Their studies revealed that adsorber performance could be constrained by solids flow patterns and back mixing on the stages [17]. Thus, ECA packings are investigated in the cross-current flow experiments in part 1 of this study to characterize the flow patterns of particles in packed-fluidized beds and compared to those without packings [31]. The results of part 1 demonstrate that using ECA packings in a cross-current flow reactor can optimize the flow patterns of solids and gases, leading to a progressive decrease in reactant concentration along the reactor's length and transitioning the solid flow behavior in the BFB reactor from CSTR-like to PFR-like behavior [31].

In the current part, the aim is to investigate the effect of packings on the performance of a cylindrical BFB setup that allows for a continuous counter-current flow of solids and fluidizing gas. Experimental findings demonstrate that employing packings with low void factor, such as ECA or ASB, reduces the axial dispersion of particles in the BFB, thereby approximating the behavior of a PFR.

It is important to emphasize that the ability to operate fluidized beds in PFR mode offers significant advantages, potentially providing an alternative to traditional methods such as moving bed reactors. For instance, studies by Zhou et al. [20], and Hsieh et al. [22] necessitate the use of very large particles in their chemical looping systems for H_2 production, and to prevent fluidization, they require very low fluidization velocities, resulting in larger reactor dimensions. In contrast, the current investigation introduces the concept of a packed fluidized bed as a novel approach to enhance reactor performance while avoiding these limitations. This innovative strategy not only optimizes the flow patterns of the reactor but also presents a scalable and economical solution for various industrial applications. Therefore, the findings of this study set the stage for future research and development focused on scaling-up experiments and economic validations. A key consideration for application in industrial processes is the potential for mechanical failure such as breakage, for example by thermal stresses during startup and shutdown in high-temperature applications, and attrition/erosion of the packings. These challenges must be addressed by evaluation in pilot-scale units to ensure suitability for scale-up.

5.1. Limitations

A limitation of using packings in bubbling fluidized beds is the potential restriction on solids flux when low-void packings are employed,

particularly where high solids circulation rates are desired, such as in circulating fluidized bed applications like chemical looping combustion (CLC). This limitation is expected, as spherical packings have a low void factor, which hinders flow and fluidization [28].

6. Conclusion

This study explores the feasibility of enhancing the flow pattern through the analysis of RTD curves of a counter-current flow BFB towards a PFR through the application of packings, a concept referred to as packed-fluidized bed or confined fluidization. The study evaluates different parameters including fluidization numbers (15.6, and 21.9), bed heights (30 cm, and 50 cm), and packing types (ASB, ECA, and no packing). The key finding is that the incorporation of packing materials effectively reduces vertical solids back mixing within the reactor. Consequently, the E -curve in the presence of packings exhibits a shape closer to a Gaussian distribution, indicative of a system behavior more alike to that of a PFR. Additional conclusions drawn from this investigation are as follows:

- The utilization of ASB and ECA packings consistently results in a substantial increase in the Peclet number (Pe) across all investigated scenarios, exhibiting up to a tenfold increase compared to unpacked configurations.
- Analysis employing the tank-in-series model reveals a significant increase, up to ninefold, in the number of tanks (N) for experiments utilizing packing compared to unpacked beds.
- Implementation of the RTD model demonstrates up to 71 % reduction in the mean residence time of tracer (τ) in the packed-fluidized bed.
- Furthermore, the RTD model demonstrates a tenfold reduction in the vessel dispersion number (D/uL) within the relevant PFR for the packed bed in contrast to the unpacked bed. Consequently, the level of axial dispersion in the system is much larger for the unpacked bubbling bed.
- The axial dispersion coefficient decreases from approximately 0.06 m^2/s in the unpacked bed to 0.006 m^2/s in the packed-fluidized bed, representing an almost tenfold reduction.

Nomenclature

A	s Area under the $C_{response}$ curve
Ar	– Archimedes number
C	– Normalized tracer concentration
$C_{response}$	– Normalized detected tracer concentration leaving the reactor
D	m^2/s Axial dispersion coefficient
D_v	m Vessel diameter
D/uL	– Vessel dispersion number ($1/Pe$)
d_p	μm Average particle diameter
E	s^{-1} Exit age distribution
F	– Fluidization number
F_s	kg/s Solid recirculation
H	m Settled bed height
L	m Length
m_s	kg Mass of solid in the bed
m_t	kg Mass of tracer
N	– Number of tanks in series
Pe	– Peclet number
t	s Time
u_{mf}	m/s Minimum fluidization velocity

Greek letters

ρ_b	kg/m^3 Bulk density of particles
ρ_p	kg/m^3 Particle density

σ^2	s^2 Variance of tracer curve
σ_0^2	– Normalized variance of tracer curve
$\tau_0 = 0$	s Beginning of each experiment at which the tracer is injected into the FB.
τ_1	s Time lag until the detection of the tracer at the outlet coil.
τ	s Mean residence time of tracer in the FB.

CRediT authorship contribution statement

Nasrin Nemati: Methodology, Investigation, Conceptualization, Writing – review & editing, Writing – original draft, Visualization, Validation, Formal analysis, Data curation. **Tobias Mattisson:** Conceptualization, Writing – review & editing, Visualization, Validation, Methodology. **David Pallarès:** Validation, Methodology, Writing – review & editing, Visualization. **Diana Carolina Guío-Pérez:** Writing – review & editing, Visualization, Validation, Methodology. **Magnus Rydén:** Writing – review & editing, Visualization, Validation, Supervision, Software, Resources, Project administration, Methodology, Funding acquisition, Conceptualization.

Declaration of competing interest

The authors declare that they have no known competing financial interests or personal relationships that could have appeared to influence the work reported in this paper.

Acknowledgements

This work has been supported by the Swedish Research Council (project 46525-1 - The application of confined fluidization in energy conversion), and the Swedish Energy Agency (P2022-00544 – production of hydrogen and biochar from wood fuels with a new process that utilizes the steam-iron reaction and iron ore concentrate).

Appendix A. Supplementary data

Supplementary data to this article can be found online at <https://doi.org/10.1016/j.powtec.2025.121306>.

Data availability

Data will be made available on request.

References

- [1] J.B. Joshi, L.K. Doraiswamy, Chemical reaction engineering, in: Albright's Chemical Engineering Handbook 38, 2008, pp. 737–968, <https://doi.org/10.1201/9781420087567-13>.
- [2] O. Levenspiel, Tracer Technology vol. 96, New York, NY, Springer New York, 2012, <https://doi.org/10.1007/978-1-4419-8074-8>.
- [3] H.S. Fogler, Elements of Chemical Reaction Engineering, Prentice Hall PTR, Upper Saddle River, N.J., 1999.
- [4] N. Nemati, R. Zarghami, N. Mostoufi, Investigation of hydrodynamics of high-temperature fluidized beds by pressure fluctuations, Chem. Eng. Technol. 39 (2016) 1527–1536, <https://doi.org/10.1002/ceat.201500443>.
- [5] G. Hofer, G. Schöny, T. Pröll, Acting on hydrodynamics to improve the local bed-to-wall heat transfer in bubbling fluidized beds, Chem. Eng. Res. Des. 134 (2018) 309–318, <https://doi.org/10.1016/j.cherd.2018.04.015>.
- [6] D. Geldart, Fluidization engineering, Powder Technol. 3 (1969) 255–256, [https://doi.org/10.1016/0032-5910\(69\)80087-2](https://doi.org/10.1016/0032-5910(69)80087-2).
- [7] D. Geldart, Types of gas fluidization, Powder Technol. 7 (1973) 285–292, [https://doi.org/10.1016/0032-5910\(73\)80037-3](https://doi.org/10.1016/0032-5910(73)80037-3).
- [8] S. Andersson, F. Johnsson, B. Leckner, Fluidization regimes in non-slugging fluidized beds, in: Proc West Mark Ed Assoc Conf, 1989, pp. 239–242.
- [9] J. Yerushalmi, High Velocity Fluidization. Fluidization, 1985, pp. 225–289.
- [10] J. Aronsson, D. Pallarès, A. Lyngfelt, Modeling and scale analysis of gaseous fuel reactors in chemical looping combustion systems, Particuology 35 (2017) 31–41, <https://doi.org/10.1016/j.partic.2017.02.007>.
- [11] J. Aronsson, E. Krymarys, V. Stenberg, T. Mattisson, A. Lyngfelt, M. Rydén, Improved gas–solids mass transfer in fluidized beds: confined fluidization in chemical-looping combustion, Energy Fuel 33 (2019) 4442–4453, <https://doi.org/10.1021/acs.energyfuels.9b00508>.

- [12] K.M. Merrett, K.J. Whitty, Conversion of coal in a fluidized bed chemical looping combustion reactor with and without oxygen uncoupling, *Energy Fuel* 33 (2019) 1547–1555, <https://doi.org/10.1021/acs.energyfuels.8b03581>.
- [13] V. Stenberg, M. Rydén, T. Mattisson, A. Lyngfelt, Exploring novel hydrogen production processes by integration of steam methane reforming with chemical-looping combustion (CLC-SMR) and oxygen carrier aided combustion (OCAC-SMR), *Int. J. Greenhouse Gas Control* 74 (2018) 28–39, <https://doi.org/10.1016/j.ijggc.2018.01.008>.
- [14] M. Rydén, A. Lyngfelt, Using steam reforming to produce hydrogen with carbon dioxide capture by chemical-looping combustion, *Int. J. Hydrog. Energy* 31 (2006) 1271–1283, <https://doi.org/10.1016/j.ijhydene.2005.12.003>.
- [15] T. Pröll, G. Schöny, G. Sprachmann, H. Hofbauer, Introduction and evaluation of a double loop staged fluidized bed system for post-combustion CO₂ capture using solid sorbents in a continuous temperature swing adsorption process, *Chem. Eng. Sci.* 141 (2016) 166–174, <https://doi.org/10.1016/j.ces.2015.11.005>.
- [16] J. Pirklbauer, G. Schöny, F. Zerobin, T. Pröll, H. Hofbauer, Optimization of stage numbers in a multistage fluidized bed temperature swing adsorption system for CO₂ capture, *Energy Procedia* 114 (2017) 2173–2181, <https://doi.org/10.1016/j.egypro.2017.03.1354>.
- [17] C. Eder, *Solids Mixing and Wall-to-Bed Heat Transfer in Cross-Flow Bubbling Fluidized Bed Reactors with Different Immersed Tube Bundles*, University of Natural Resources and Life Science, Vienna, 2021.
- [18] Z. Xue, S. Chen, D. Wang, W. Xiang, Design and fluid dynamic analysis of a three-fluidized-bed reactor system for chemical-looping hydrogen generation, *Ind. Eng. Chem. Res.* 51 (2012) 4267–4278, <https://doi.org/10.1021/ie201052r>.
- [19] S. Chen, Z. Xue, X. Wang, C. Xu, D. Wang, W. Xiang, Reduction Behavior of Iron Oxide for Chemical-Looping Hydrogen Generation in a Compact Fluidized Fuel Reactor Vol. 6A, *Energy*, American Society of Mechanical Engineers, 2014, <https://doi.org/10.1115/IMECE2014-36204>.
- [20] Q. Zhou, L. Zeng, L. Fan, Syngas chemical looping process: dynamic modeling of a moving-bed reducer, *AIChE J.* 59 (2013) 3432–3443, <https://doi.org/10.1002/aic.14181>.
- [21] D. Wang, L. Fan, Bulk coarse particle arching phenomena in a moving bed with fine particle presence, *AIChE J.* 60 (2014) 881–892, <https://doi.org/10.1002/aic.14320>.
- [22] T.-L. Hsieh, Y. Zhang, D. Xu, C. Wang, M. Pickarts, C. Chung, et al., Chemical looping gasification for producing high purity, H₂-rich syngas in a Cocurrent moving bed reducer with coal and methane cofeeds, *Ind. Eng. Chem. Res.* 57 (2018) 2461–2475, <https://doi.org/10.1021/acs.iecr.7b04204>.
- [23] M. Farha, D.C. Guío-Pérez, F. Johnsson, D. Pallarès, Characterization of the solids crossflow in a bubbling fluidized bed, *Powder Technol.* 443 (2024) 119967, <https://doi.org/10.1016/j.powtec.2024.119967>.
- [24] N. Nemati, M. Rydén, Chemical-looping combustion in packed-fluidized beds: experiments with random packings in bubbling bed, *Fuel Process. Technol.* 222 (2021) 106978, <https://doi.org/10.1016/j.fuproc.2021.106978>.
- [25] N. Nemati, Y. Tsuji, T. Mattisson, M. Rydén, Chemical looping combustion in a packed fluidized bed reactor—fundamental Modeling and batch experiments with random metal packings, *Energy Fuel* (2022), <https://doi.org/10.1021/acs.energyfuels.2c00527>.
- [26] N. Nemati, P. Andersson, V. Stenberg, M. Rydén, Experimental investigation of the effect of random packings on heat transfer and particle segregation in packed-fluidized bed, *Ind. Eng. Chem. Res.* 60 (2021) 10365–10375, <https://doi.org/10.1021/acs.iecr.1c01221>.
- [27] J. Aronsson, D. Pallarès, M. Rydén, A. Lyngfelt, Increasing gas–solids mass transfer in fluidized beds by application of confined fluidization—a feasibility study, *Appl. Sci.* 9 (2019) 634, <https://doi.org/10.3390/app9040634>.
- [28] N. Nemati, P. Filiu Moreno, M. Rydén, Investigation of the hydrodynamics of packed-fluidized beds: characterization of solids flux, *Fuel* 335 (2023) 127010, <https://doi.org/10.1016/j.fuel.2022.127010>.
- [29] A. Lyngfelt, B. Leckner, A 1000 MWth boiler for chemical-looping combustion of solid fuels – discussion of design and costs, *Appl. Energy* 157 (2015) 475–487, <https://doi.org/10.1016/j.apenergy.2015.04.057>.
- [30] G. Hofer, T. Märzinger, C. Eder, F. Pröll, T. Pröll, Particle mixing in bubbling fluidized bed reactors with continuous particle exchange, *Chem. Eng. Sci.* 195 (2019) 585–597, <https://doi.org/10.1016/j.ces.2018.10.001>.
- [31] N. Nemati, T. Pröll, T. Mattisson, M. Rydén, Impact of random packing on residence time distribution of particles in bubbling fluidized beds: Part 1—cross-current flow reactors, *Chem. Eng. Sci.* (2024) 120724, <https://doi.org/10.1016/j.ces.2024.120724>.
- [32] D.C. Guío-Pérez, T. Pröll, J. Wassermann, H. Hofbauer, Design of an Inductance Measurement System for determination of particle residence time in a dual circulating fluidized bed cold flow model, *Ind. Eng. Chem. Res.* 52 (2013) 10732–10740, <https://doi.org/10.1021/ie400211h>.
- [33] C. Eder, G. Hofer, J. Beer, T. Pröll, Particle mixing in bubbling fluidized bed reactors with immersed heat exchangers and continuous particle exchange, *Ind. Eng. Chem. Res.* 59 (2020) 19736–19750, <https://doi.org/10.1021/acs.iecr.0c03568>.